Title

Controlled CO labilization of tungsten carbonyl precursors for the low-temperature synthesis of tungsten diselenide nanocrystals

Authors

Geisenhoff, Jessica Q

Yin, Hang

Oget, Natacha

et al.

Publication Date

2022

DOI

10.3389/fnano.2022.1026635

Peer reviewed

Controlled CO Labilization of Tungsten Carbonyl Precursors for the Low-Temperature Synthesis of Tungsten Diselenide Nanocrystals

Jessica Q. Geisenhoff[†], Hang Yin[†], Natacha Oget, Haeun Chang, Linfeng Chen and Alina M. Schimpf*

Department of Chemistry and Biochemistry, University of California, San Diego, La Jolla, CA 92093, USA
**Electronic address: aschimpf@ucsd.edu*

[†]These authors contributed equally

Abstract. We report a low-temperature colloidal synthesis of WSe_2 nanocrystals from tungsten hexacarbonyl and diphenyl diselenide in trioctylphosphine oxide (TOPO). We identify TOPO-substituted intermediates, $W(CO)_5$TOPO and *cis*-$W(CO)_4(TOPO)_2$ by infrared spectroscopy. To confirm these assignments, we synthesize aryl analogues of phosphine-oxide-substituted intermediates, $W(CO)_5$TPPO (synthesized previously, TPPO = triphenylphosphine oxide) and *cis*-$W(CO)_4(TPPO)_2$ and *fac*-$W(CO)_3(TPPO)_3$ (new structures reported herein). Ligation of the tungsten carbonyl by either the alkyl or aryl phosphine oxides results in facile labilization of the remaining CO, enabling low-temperature decomposition to nucleate WSe_2 nanocrystals. The reactivity in phosphine oxides is contrasted with syntheses containing phosphine ligands, where substitution results in decreased CO labilization and higher temperatures are required to induce nanocrystal nucleation.

Colloidal synthesis provides an attractive route to solid-state nanomaterials because it can exploit the diverse reaction-parameter-space to obtain kinetic control, enabling access to products that are difficult or impossible to achieve via bulk synthetic methods. Understanding and manipulating the precursor chemistry has emerged as a vital tool for advancing nanocrystal syntheses, as precursor conversion governs the nucleation and growth of nanocrystals.[1-5] Differences in precursor reactivity have been used to tailor nanocrystal size,[6-9] morphology[10-12] and phase.[11, 13-20] For example, the size and size-distributions of cadmium, lead, and zinc chalcogenides have been greatly tuned via a selection of thioureas and selenoureas to vary the kinetics of the chalcogen supply.[6-9] The shape of copper nanocrystals has been selected through manipulation of the ligand-bound copper intermediate to vary the rate of conversion to active monomers. Ligation with trioctylphosphine oxide results in rapid conversion and the kinetically favored cubic product, while trioctylphosphine yields the thermodynamically favored spherical nanocrystals.[10] In the synthesis of WSe_2 nanocrystals,[18, 20] inclusion of trioctylphosphine oxide, oleic acid or oleylamine ligands was shown to vary the precursor reactivity, concomitant with a change in the phase of the final products. We hypothesize that differences in the observed reactivity

are due to differences in the decomposition of the tungsten carbonyl precursors, where substitution by ligands at the metal center serves to modulate the energy required for dissociation.

Metal carbonyls, including tungsten hexacarbonyl,[18, 20-27] molybdenum hexacarbonyl,[22, 28-30] iron pentacarbonyl¸[31-35] dicobalt octacarbonyl,[32, 36-39] and dimanganese decacarbonyl[33, 40-42] are widely used in the solution-phase syntheses of metal,[21, 23-26, 29, 32, 36-41] metal carbide,[30, 35] metal phosphide[31] or metal chalcogenide nanocrystals, [18, 20, 22, 27-29, 33-34] where they are commonly used as a source of metal[18, 20-22, 27-28, 31-34, 36, 38-41] or as a reducing agent.[23-26, 37, 42] The use of metal carbonyl precursors generally requires temperatures high enough to force cleavage of the metal–carbonyl bonds[43] and induce nanocrystal nucleation. Metal carbonyls can decompose directly to form metal nanocrystals,[21, 32, 36, 38-40] or can undergo ligand exchange at the metal site.[44-48] Such ligand exchange is expected to be important in controlling the subsequent reactivity of the metal carbonyls, but its role in nanocrystal formation has not been explicitly explored. As CO alone has been shown to direct nanocrystal growth and morphology,[49-50] its labilization from metal carbonyls can also be expected to influence nanocrystal formation. Here, we show that the ligands/solvents common in many nanocrystal syntheses play an important role in forming and dictating the reactivity of substituted tungsten carbonyls that are used to form WSe_2 nanocrystals.

We have previously synthesized WSe_2 nanocrystals by hot-injection of diphenyl diselenide (Ph_2Se_2) into tungsten hexacarbonyl ($W(CO)_6$) dissolved in mixtures of trioctylphosphine oxide (TOPO) and oleic acid (OA) at 330 °C.[18] When using this mixture of ligands, the reactivity is increased with a larger TOPO/OA ratio, leading to more nanocrystal nucleation and smaller nanocrystals that are readily converted to the thermodynamically favored phase.[18] Indeed, when OA is excluded, $W(CO)_6$ decomposes at 260 °C, prior to injection of Ph_2Se_2.[18] Here, we take advantage of this greater reactivity in TOPO by using a low-temperature injection of Ph_2Se_2 to form WSe_2 nanocrystals at 150 °C. We follow the reactivity and conversion of $W(CO)_6$ using IR spectroscopy and show that, prior to Ph_2Se_2 injection, one or two CO ligands are replaced by TOPO ligands, enabling facile CO labilization. In contrast, when just one eq trioctylphosphine (TOP) is included, the TOP-substituted tungsten carbonyl is exclusively formed. This intermediate has decreased ligand dissociation from the tungsten, such that nanocrystals cannot be nucleated below 180 °C. The assignment of the phosphine- and phosphine-oxide-substituted intermediates is verified by synthesis of the aryl analogs (TPP and TPPO, respectively; TPP = triphenylphosphine, TPPO = triphenylphosphine oxide), which can be crystallized for structural identification. These

studies demonstrate the role that phosphines and phosphine oxides can play in nanocrystal nucleation and growth by dictating the conversion of metal carbonyl precursors.

Results and Analysis

WSe_2 nanocrystals were synthesized via injection of Ph_2Se_2 into $W(CO)_6$ dissolved in TOPO at 150 °C. Briefly, $W(CO)_6$ (20 mg, 0.057 mmol) was heated in TOPO (2.1975 g, 100 TOPO/W) to 150 °C and held for 15 min. Beginning at ~ 70° C, the colorless solution began to turn yellow and continued to darken as the temperature increased. This color change was accompanied by bubbling, indicative of some gas evolution. After 15 min at 150 °C, Ph_2Se_2 in hexadecane (115 mM, 1 ml, 4 Se/W) was rapidly injected into the W solution. Immediately after injection, the solution changed to brown/black and rapid gas evolution was observed, indicating nucleation of WSe_2 nanocrystals.

Figure 1a(0) shows the IR spectrum of an aliquot collected just before the Ph_2Se_2 injection. Here, multiple CO vibrations are observed between 1950 and 1850 cm^{-1} (Table S1). These vibrations are all shifted to lower wavenumber relative to that of $W(CO)_6$ (1971 cm^{-1}, Figure S1), suggesting that $W(CO)_6$ has undergone substitution by TOPO to form $W(CO)_{6-x}(TOPO)_x$ intermediates. Similar shifts are observed when the CO of $W(CO)_6$ is substituted by one, two or three phosphine oxide ligands.[51-53] Just one minute following Ph_2Se_2 injection, the original peaks disappear and are replaced by weak vibrations at 1937 and 1903 cm^{-1} (Figure 1a(i)), which likely arise from another intermediate formed by oxidative addition of Ph_2Se_2 to the $W(CO)_{6-x}(TOPO)_x$ complexes.[54-56] Within 10 min following Ph_2Se_2 injection, no CO vibrations are evident in the IR spectrum (Figure 1a(iii)), indicating complete conversion of the $W(CO)_{6-x}(TOPO)_x$ intermediates. The heating profile of this synthesis is provided in Figure 1b, with the x indicating nucleation and filled circles indicating when aliquots were taken. After 10 min following Ph_2Se_2 injection, the heating mantle was removed and the resultant nanocrystals were collected, washed and characterized.

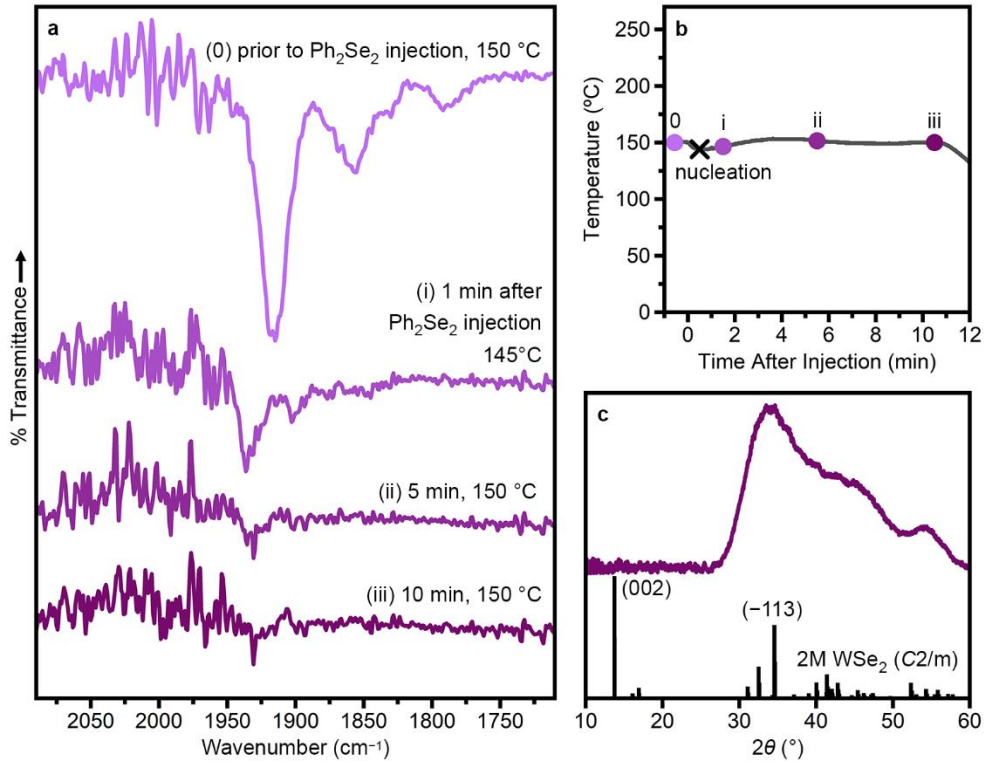

Figure 1. Injection of Ph_2Se_2 into $W(CO)_6$ + TOPO (TOPO/Se/W = 100/4/1) at 150 °C. **(a)** FTIR spectra of aliquots taken prior to Se injection and approximately 1, 5 and 10 min after Se injection. **(b)** Temperature profile of the reaction with aliquots indicated by circles. The black x indicates the nucleation event, evidenced by a color-change of the reaction solution. **(c)** Powder X-ray diffraction pattern of nanocrystalline product compared to that simulated from single-crystal data for 2M WSe_2.[57]

Figure 1c shows the powder X-ray diffraction pattern of the resulting nanocrystals. The lack of a (002) reflection suggests very little interlayer stacking, which is confirmed by transmission electron microscopy (Figure S2). The most intense reflection is observed at $2\theta \approx 34°$, consistent with the (−113) reflection of the metastable 2M phase of WSe_2.[18, 27, 57] This phase-assignment is verified by X-ray photoelectron spectroscopy (Figure S3). We have previously shown that increased TOPO/OA leads to more 2H phase when WSe_2 nanocrystals are synthesized at 330 °C.[18] In this previous work, dominance of the thermodynamically favored phase was due to greater reactivity induced by TOPO, which led to more phase-conversion at high temperatures.[18] In contrast, the synthesis presented herein takes advantage of the TOPO-induced reactivity to synthesize WSe_2 nanocrystals at lower temperatures, allowing preservation of the metastable 2M phase.

Since the bulky octyl groups of TOPO prohibit the isolation of single crystals, we used an aryl analog to corroborate the formation of $W(CO)_{6-x}(TOPO)_x$ intermediates. Specifically, we synthesized $W(CO)_{6-x}(TPPO)_x$ (x = 1, 2, 3). $W(CO)_5TPPO$ (Figure 2a) was synthesized from photochemically prepared $W(CO)_5THF$ (THF = tetrahydrofuran) following a previously reported procedure.[51] To synthesize $W(CO)_4(TPPO)_2$, $W(CO)_6$ and TPPO (10 eq) were combined in toluene and refluxed for ~1 h with stirring. Further addition of toluene resulted in a yellow precipitate, which was redissolved with heat. The resulting solution yielded yellow crystals in ~12 h. Single-crystal X-ray diffraction identified the crystals as *cis*-$W(CO)_4(TPPO)_2$ (Figure 2b, Table S2) and powder X-ray diffraction confirmed this as the majority product (Figure S4). We note, however, that a trace product of *fac*-$W(CO)_3(TPPO)_3$ (Table S2, Figure S5) was identified by single-crystal X-ray diffraction.

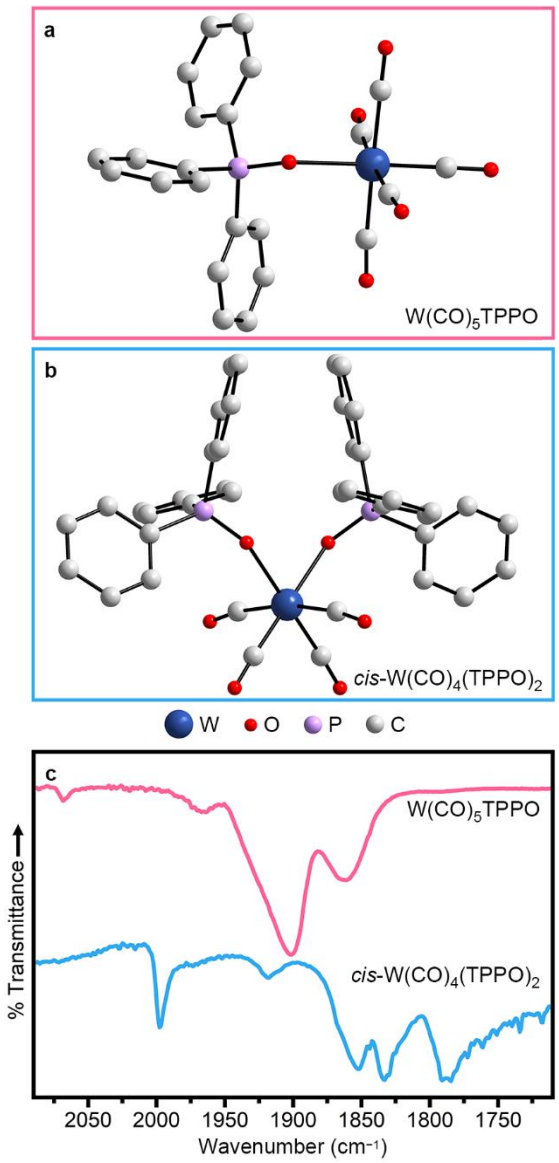

Figure 2. Crystal structures of **(a)** $W(CO)_5TPPO$ and **(b)** *cis*-$W(CO)_4(TPPO)_2$. **(c)** FTIR spectra of $W(CO)_5TPPO$ (top) and of *cis*-$W(CO)_4(TPPO)_2$ (bottom) solids.

Figure 2c (top, pink) shows the IR spectrum of $W(CO)_5TPPO$. With pseudo-C_{4v} symmetry, this molecule has 4 IR-active CO vibrations (Table S3).[51, 53] Figure 2c (bottom, blue) shows the IR spectrum of *cis*-$W(CO)_4(TPPO)_2$. With pseudo-C_{2v} symmetry, this molecule also has 4 IR-active CO vibrations (Table S4), which are at similar positions to other tungsten carbonyls substituted with two phosphine oxide moieties.[52] Comparing the IR spectra of these two molecules to that of the pre-injection aliquot (Figure 1a(0)), we conclude that heating $W(CO)_6$ in TOPO yields a mixture of the mono- and di-substituted species, $W(CO)_5TOPO$ and *cis*-$W(CO)_4(TOPO)_2$, respectively (Table S1). The lack of a peak at ~1970 cm^{-1} indicates little to no remaining $W(CO)_6$,

suggesting that $W(CO)_5TOPO$ and *cis*-$W(CO)_4(TOPO)_2$ are the reactive intermediates when Ph_2Se_2 is injected. Phosphine oxides are known to be particularly good at promoting CO labilization in metal carbonyls,[45, 58-59] which is likely the reason for increased reactivity when WSe_2 nanocrystals are synthesized in TOPO.

It is worth noting that both increased concentration of $W(CO)_6$ (Figure S6) and the addition of a degassing step (Figure S7) leads to more substitution by TOPO. When the synthesis is repeated using TPPO instead of TOPO, the reactivity is similar. Specifically, nucleation was observed immediately after the injection of Ph_2Se_2 and WSe_2 nanocrystals are formed within 10 min at 150 °C (Figure S8). These observations corroborate that the higher reactivity is due to the phosphine oxides.

To contrast the rapid reactivity induced by TOPO, we sought a ligand with stronger binding and decreased CO labilization that would decrease reactivity in the nanocrystal synthesis. TOP is commonly used in nanocrystal syntheses and contains a strong σ-donating, π-accepting phosphine in contrast to the weak, hard oxygen donor of TOPO. Figure 3 shows the characterization of a WSe_2 synthesis performed similarly to that presented in Figure 1, but with just 1 eq TOP added to the reaction mixture. When $W(CO)_6$ is heated at 150 °C in the presence of 100 eq TOPO + 1 eq TOP for 15 min, IR spectroscopy reveals a new species (Figure 3a(0)), with vibrations that are distinct from both $W(CO)_6$ and $W(CO)_{6-x}(TOPO)_x$. We assign this species as primarily $W(CO)_5TOP$ with a small amount of $W(CO)_4(TOP)_2$ (Table S5, *vide infra*). Importantly, when Ph_2Se_2 is injected into this mixture at 150 °C, no color change or gas evolution are observed over the course of 11 min and the CO vibrations remain largely unchanged (Figure 3a(i–iii)).

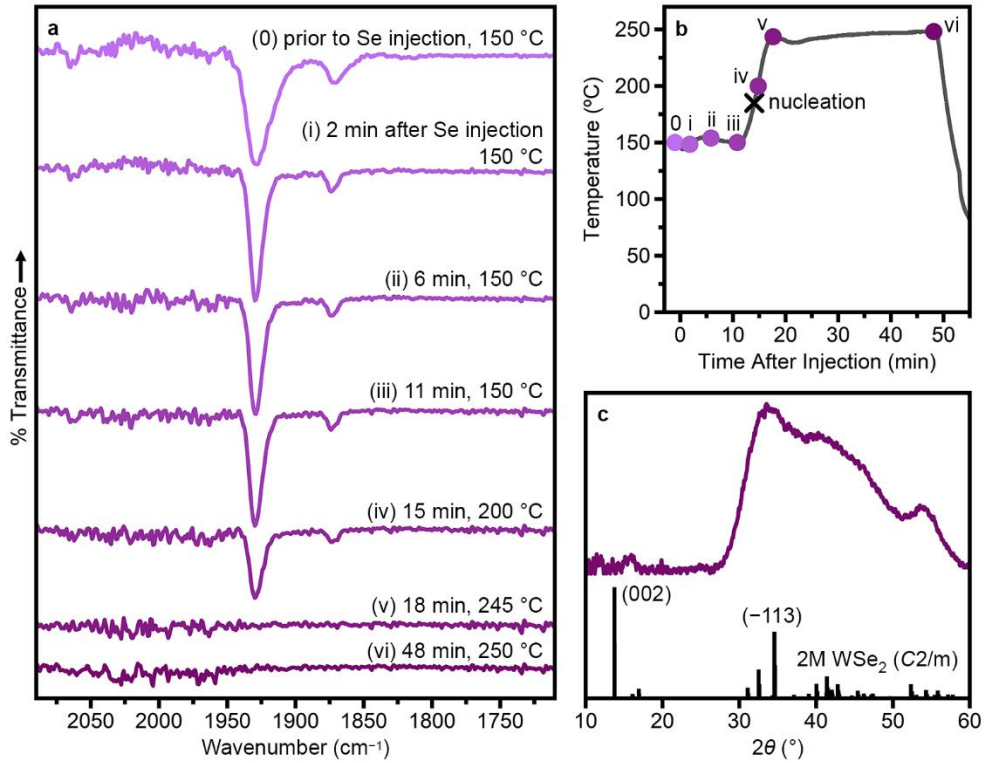

Figure 3. Injection of Ph_2Se_2 into $W(CO)_6$ + TOPO + TOP (TOPO/TOP/Se/W = 100/1/4/1) at 150 °C. **(a)** FTIR spectra of aliquots taken prior to Se injection and approximately 2, 6, 11, 15, 18 and 48 min after Se injection. **(b)** Temperature profile of the reaction with aliquots indicated by circles. The black x indicates the nucleation event, evidenced by a color-change of the reaction solution. **(c)** Powder X-ray diffraction pattern of nanocrystalline product compared to that simulated from single-crystal data for 2M WSe_2.[57]

The low reactivity in the presence of TOP is in stark contrast to syntheses without TOP, in which a color-change, gas evolution and loss of CO are observed immediately upon injection (Figure 1a, b). To induce nanocrystal nucleation, the reaction was heated to 250 °C over ~10 min (Figure 3b). As the temperature was increased, the solution began to turn brown, indicating nucleation of WSe_2. This color-change was accompanied by gas evolution, indicating liberation of CO. When the temperature reached 250 °C, the solution was very dark brown and gas evolution had slowed. Aliquots were collected shortly after nucleation (Figure 3a,b(iv)), once the temperature reached 250 °C (Figure 3a,b(v) and after 30 min at 250 °C (Figure 3a,b(vi)). The intensity of the $W(CO)_5$TOP CO vibration at 1930 cm^{-1} decreased following WSe_2 nucleation, and disappeared completely by the time the temperature reached 250 °C. Powder X-ray diffraction (Figure 3c) on the final nanocrystalline product reveals 2M WSe_2.

To confirm the assignment of $W(CO)_5TOP$, we synthesized the aryl analog, $W(CO)_5TPP$ (Figure 4a) using previously reported methods.[60] Figure 4b(i) shows the IR spectrum of crystals of $W(CO)_5TPP$ dissolved in THF. With pseaudo-C_{4v} symmetry, this molecule is expected to have 4 IR-active CO vibrations, but in this case the $A_1(2)$ and E modes are unresolvable (Table S6).[61-62] Importantly, when $W(CO)_5TPP$ is heated in 100 eq TOPO at 150 °C for 15 min (Figure 4b(ii)), the IR spectrum is comparable to that of the TOP-containing syntheses prior to injection of Ph_2Se_2 (Figure 3a(0)), and can be assigned primarily to $W(CO)_5TPP$ with a small amount of $W(CO)_4(TPP)_2$ (Table S7). All peaks are shifted to slightly higher wavenumber for TPP-substituted species relative to the TOP-substituted species due to the electron-withdrawing nature of the phenyl substituents.[63-64]

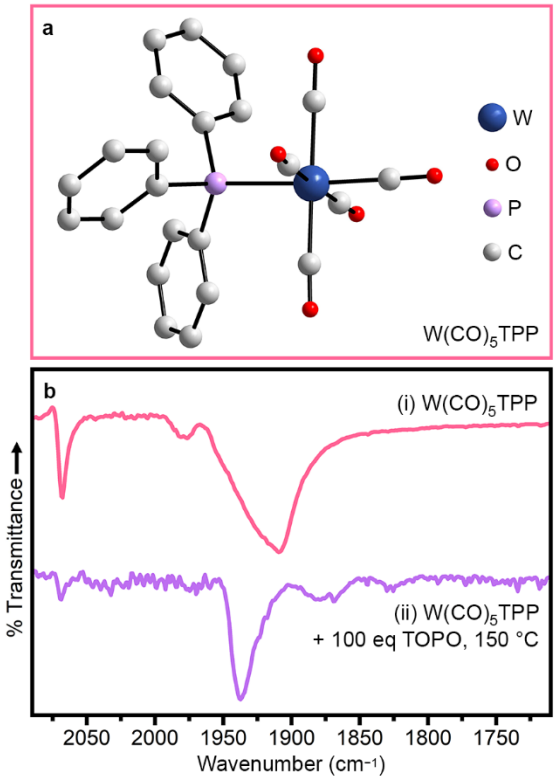

Figure 4. (a) Crystal structure of $W(CO)_5TPP$. **(b)** IR spectra of (i) $W(CO)_5TPP$ dried solid and of (ii) that solid heated in 100 eq TOPO to 150 °C for 15 min (bottom). All spectra were collected at room-temperature.

When Ph_2Se_2 is injected into $W(CO)_5TPP$ + 100 eq TOPO at 150 °C, the reactivity is similar to that of the TOP-containing synthesis. Specifically, no color-change or gas evolution were observed over 10 min and the $W(CO)_5TPP$ CO vibration at 1937 cm^{-1} persisted, although with

some decrease in intensity. We note that, in this synthesis, the CO vibration assigned to $W(CO)_4(TPP)_2$ disappears upon injection of Ph_2Se_2. We hypothesize that this is due to conversion of $W(CO)_4(TPP)_2$ to $W(CO)_5TPP$. This conversion results in formation of a small amount of TPP=Se and Ph_2Se (equation S1), neither of which can react directly with $W(CO)_5TPP$ to nucleate nanocrystals at 150 °C. When the reaction is further heated, a color change is observed, indicating nucleation of WSe_2 (Figure S9b). The reactivity of $W(CO)_5TPP$ is greater than that of the TOP-containing synthesis, likely due to the electron-withdrawing nature of the phenyl substituents. Both phosphine-substituted species, however, show delayed reactivity compared to synthesis in TOPO alone. This observation confirms that carbonyl substitution with phosphines or phosphine oxides can be used to delay or induce nanocrystal nucleation, respectively.

Discussion

The decrease in reactivity observed with the phosphine substitution compared to phosphine-oxide substitution is likely two-fold. First, the phosphine is a stronger σ-donating and π-accepting ligand, making it less labile than the phosphine oxide ligand.[65] Second, phosphine- and phosphite-substitution in metal carbonyls have been shown to decrease CO labilization.[44, 46-48, 59, 66-69] In contrast, substitution with hard donor ligands,[44, 46, 48, 67-68, 70] including phosphine oxides,[45, 58-59] has been shown to increase CO labilization in metal carbonyls. This has been explained due to σ- and π-bonding effects between the donor and central metal atom, as well as a result of direct donation from the filled σ_z^b orbital of the donor to the π* orbitals of the carbonyls cis to the donor.[48, 68, 71] The low lability of both the phosphine and carbonyl ligands inhibits coordination by the Se precursor, thus requiring higher temperatures to force cleavage of the W–C and/or W–P bonds to initiate WSe_2 nucleation. We note that the substituents of the phosphine ligand also play a significant role in modifying the reactivity of the substituted metal carbonyls. With direct coordination to the donor, electron-withdrawing groups (e.g. phenyl substituents) decrease the P–W bond strength to allow for ligand dissociation at lower temperatures. This effect is not present in the phosphine oxides, as the substituents are not well-coupled to the donor.

In our hands, $W(CO)_6$ does not dissolve well in noncoordinating solvents used for nanocrystal synthesis, such as hexadecane. Thus, the influence on reactivity of a coordinating solvent will likely be an important consideration. The reactivity trend observed with phosphine oxides vs

phosphines can possibly be extended to other common nanocrystal ligands/solvents based on the known reactivity with metal carbonyls. For example, oleylamine would also be expected to be CO-labilizing due to the hard N donor, [44, 46, 48, 67-68, 70] and could facilitate metal carbonyl decomposition.[24] Variation of the substituents on the N donor could be used to further tune the reactivity. We note that we have not discussed the role of steric interactions, which could be used to further modify the metal carbonyl stability.

Summary and Conclusions

We present a low-temperature synthesis of WSe_2 nanocrystals by taking advantage of the modified reactivity of substituted tungsten carbonyls. When nanocrystals are synthesized in TOPO, $W(CO)_5$TOPO and *cis*-$W(CO)_4(TOPO)_2$ are identified as the reactive tungsten intermediates. This substitution with TOPO enables facile CO labilization, allowing for the ligand dissociation required to initiate reactivity of the tungsten carbonyls with the Se precursor at 150 °C. In contrast, when just 1 eq TOP is included, nanocrystals cannot be nucleated below 180 °C due to the non-labilizing nature of the phosphine. The reactivity of phosphine-containing syntheses can be further tuned via choice of phosphine substituent, where electron-withdrawing groups lead to increased reactivity. These results demonstrate the influence of common nanocrystal ligands on metal carbonyl reactivity and offer insight for fine-tuning the reactivity to manipulate nanocrystal nucleation and growth.

Supporting Information Available

Supplementary figures and tables; experimental details including synthesis and characterization methods; CIFs for *cis*-$W(CO)_4(TOPO)_2$ and *fac*-$W(CO)_3(TOPO)_3$.

Acknowledgements

This research was supported by the U. S. National Science Foundation (CHE-2003675 to A.M.S.). XPS data were collected at the UC Irvine Materials Research Institute using instrumentation funded in part by the National Science Foundation Major Research Instrumentation Program (CHE-1338173).

References

1. Liu, H. T.; Owen, J. S.; Alivisatos, A. P. Mechanistic Study of Precursor Evolution in Colloidal Group II–VI Semiconductor Nanocrystal Synthesis. *J. Am. Chem. Soc.* **2007,** *129*, 305.
2. Steckel, J. S.; Yen, B. K. H.; Oertel, D. C.; Bawendi, M. G. On the Mechanism of Lead Chalcogenide Nanocrystal Formation. *J. Am. Chem. Soc.* **2006,** *128*, 13032.
3. Garcia-Rodriguez, R.; Liu, H. T. Mechanistic Study of the Synthesis of CdSe Nanocrystals: Release of Selenium. *J. Am. Chem. Soc.* **2012,** *134*, 1400.
4. Owen, J. S.; Chan, E. M.; Liu, H. T.; Alivisatos, A. P. Precursor Conversion Kinetics and the Nucleation of Cadmium Selenide Nanocrystals. *J. Am. Chem. Soc.* **2010,** *132*, 18206.
5. Hendricks, M. P.; Cossairt, B. M.; Owen, J. S. The Importance of Nanocrystal Precursor Conversion Kinetics: Mechanism of the Reaction between Cadmium Carboxylate and Cadmium Bis(diphenyldithiophosphinate). *ACS Nano* **2012,** *6*, 10054.
6. Bennett, E.; Greenberg, M. W.; Jordan, A. J.; Hamachi, L. S.; Banerjee, S.; Billinge, S. J. L.; Owen, J. S. Size Dependent Optical Properties and Structure of ZnS Nanocrystals Prepared from a Library of Thioureas. *Chem. Mater.* **2022,** *34*, 706.
7. Campos, M. P.; Hendricks, M. P.; Beecher, A. N.; Walravens, W.; Swain, R. A.; Cleveland, G. T.; Hens, Z.; Sfeir, M. Y.; Owen, J. S. A Library of Selenourea Precursors to PbSe Nanocrystals with Size Distributions near the Homogeneous Limit. *J. Am. Chem. Soc.* **2017,** *139*, 2296.
8. Hamachi, L. S.; Plante, I. J. L.; Coryell, A. C.; De Roo, J.; Owen, J. S. Kinetic Control over CdS Nanocrystal Nucleation Using a Library of Thiocarbonates, Thiocarbamates, and Thioureas. *Chem. Mater.* **2017,** *29*, 8711.
9. Hendricks, M. P.; Campos, M. P.; Cleveland, G. T.; Jen-La Plante, I.; Owen, J. S. A Tunable Library of Substituted Thiourea Precursors to Metal Sulfide Nanocrystals. *Science* **2015,** *348*, 1226.
10. Strach, M.; Mantella, V.; Pankhurst, J. R.; Iyengar, P.; Loiudice, A.; Das, S.; Corminboeuf, C.; van Beek, W.; Buonsanti, R. Insights into Reaction Intermediates to Predict Synthetic Pathways for Shape-Controlled Metal Nanocrystals. *J. Am. Chem. Soc.* **2019,** *141*, 16312.
11. Mantella, V.; Varandili, S. B.; Pankhurst, J. R.; Buonsanti, R. Colloidal Synthesis of Cu–M–S (M = V, Cr, Mn) Nanocrystals by Tuning the Copper Precursor Reactivity. *Chem. Mater.* **2020,** *32*, 9780.
12. Geisenhoff, J. Q.; Tamura, A. K.; Schimpf, A. M. Manipulation of Precursor Reactivity for the Facile Synthesis of Heterostructured and Hollow Metal Selenide Nanocrystals. *Chem. Mater.* **2020,** *32*, 2304.
13. Norako, M. E.; Brutchey, R. L. Synthesis of Metastable Wurtzite $CuInSe_2$ Nanocrystals. *Chem. Mater.* **2010,** *22*, 1613.
14. Tappan, B. A.; Barim, G.; Kwok, J. C.; Brutchey, R. L. Utilizing Diselenide Precursors toward Rationally Controlled Synthesis of Metastable $CuInSe_2$ Nanocrystals. *Chem. Mater.* **2018,** *30*, 5704.
15. Hernandez-Pagan, E. A.; Robinson, E. H.; La Croix, A. D.; Macdonald, J. E. Direct Synthesis of Novel $Cu_{2-x}Se$ Wurtzite Phase. *Chem. Mater.* **2019,** *31*, 4619.
16. Rhodes, J. M.; Jones, C. A.; Thal, L. B.; Macdonald, J. E. Phase-Controlled Colloidal Syntheses of Iron Sulfide Nanocrystals via Sulfur Precursor Reactivity and Direct Pyrite Precipitation. *Chem. Mater.* **2017,** *29*, 8521.

17. Lord, R. W.; Fanghanel, J.; Holder, C. F.; Dabo, I.; Schaak, R. E. Colloidal Nanoparticles of a Metastable Copper Selenide Phase with Near-Infrared Plasmon Resonance. *Chem. Mater.* **2020,** *32*, 10227.
18. Geisenhoff, J. Q.; Tamura, A. K.; Schimpf, A. M. Using Ligands to Control Reactivity, Size and Phase in the Colloidal Synthesis of WSe_2 Nanocrystals. *Chem. Commun.* **2019,** *55*, 8856.
19. Plummer, L. K.; Hutchison, J. E. Understanding the Effects of Iron Precursor Ligation and Oxidation State Leads to Improved Synthetic Control for Spinel Iron Oxide Nanocrystals. *Inorg. Chem.* **2020,** *59*, 15074.
20. Zhou, P. S.; Schiettecatte, P.; Vandichel, M.; Rousaki, A.; Vandenabeele, P.; Hens, Z.; Singh, S. Synthesis of Colloidal WSe_2 Nanocrystals: Polymorphism Control by Precursor-Ligand Chemistry. *Cryst. Growth Des.* **2021,** *21*, 1451.
21. Sahoo, P. K.; Kamal, S. S. K.; Premkumar, M.; Kumar, T. J.; Sreedhar, B.; Singh, A. K.; Srivastava, S. K.; Sekhar, K. C. Synthesis of Tungsten Nanoparticles by Solvothermal Decomposition of Tungsten Hexacarbonyl. *Int. J. Refract. Met. H* **2009,** *27*, 784.
22. Jung, W.; Lee, S.; Yoo, D.; Jeong, S.; Miro, P.; Kuc, A.; Heine, T.; Cheon, J. Colloidal Synthesis of Single-Layer MSe_2 (M = Mo, W) Nanosheets via Anisotropic Solution-Phase Growth Approach. *J. Am. Chem. Soc.* **2015,** *137*, 7266.
23. Wang, Z. C.; Chen, Y. Z.; Zeng, D. Q.; Zhang, Q. F.; Peng, D. L. Solution Synthesis of Triangular and Hexagonal Nickel Nanosheets With the Aid of Tungsten Hexacarbonyl. *CrystEngComm* **2016,** *18*, 1295.
24. Zhao, X. X.; Di, Q.; Wu, X. T.; Liu, Y. B.; Yu, Y. K.; Wei, G. J.; Zhang, J.; Quan, Z. W. Mild Synthesis of Monodisperse Tin Nanocrystals and Tin Chalcogenide Hollow Nanostructures. *Chem. Commun.* **2017,** *53*, 11001.
25. Xiao, L.; Zhou, T.; Chen, Y. Z.; Wang, Z. C.; Zheng, H. F.; Xu, W. J.; Zeng, D. Q.; Peng, D. L. Tungsten Hexacarbonyl-Induced Growth of Nickel Nanorods and Nanocubes. *Mater. Lett.* **2018,** *229*, 340.
26. Zhao, X. X.; Di, Q.; Li, M. R.; Yang, Q.; Zhang, Z. Y.; Guo, X. Y.; Fan, X. K.; Deng, K. R.; Chen, W.; Zhang, J.; Fang, J. Y.; Quan, Z. W. Generalized Synthesis of Uniform Metal Nanoparticles Assisted with Tungsten Hexacarbonyl. *Chem. Mater.* **2019,** *31*, 4325.
27. Sokolikova, M. S.; Sherrell, P. C.; Palczynski, P.; Bemmer, V. L.; Mattevi, C. Direct Solution-Phase Synthesis of 1T′ WSe_2 Nanosheets. *Nat. Commun.* **2019,** *10*.
28. Guo, W. B.; Chen, Y. Z.; Wang, L. S.; Xu, J.; Zeng, D. Q.; Peng, D. L. Colloidal Synthesis of $MoSe_2$ Nanonetworks and Nanoflowers With Efficient Electrocatalytic Hydrogen-Evolution Activity. *Electrochim. Acta* **2017,** *231*, 69.
29. Liu, M.; Wang, Z. J.; Liu, J. X.; Wei, G. J.; Du, J.; Li, Y. P.; An, C. H.; Zhang, J. Synthesis of Few-Layer 1T'-$MoTe_2$ Ultrathin Nanosheets for High-Performance Pseudocapacitors. *J. Mater. Chem. A* **2017,** *5*, 1035.
30. Baddour, F. G.; Roberts, E. J.; To, A. T.; Wang, L.; Habas, S. E.; Ruddy, D. A.; Bedford, N. M.; Wright, J.; Nash, C. P.; Schaidle, J. A.; Brutchey, R. L.; Malmstadt, N. An Exceptionally Mild and Scalable Solution-Phase Synthesis of Molybdenum Carbide Nanoparticles for Thermocatalytic CO2 Hydrogenation. *J. Am. Chem. Soc.* **2020,** *142*, 1010.
31. Qian, C.; Kim, F.; Ma, L.; Tsui, F.; Yang, P.; Liu, J. Solution-Phase Synthesis of Single-Crystalline Iron Phosphide Nanorods/Nanowires. *J. Am. Chem. Soc.* **2004,** *126*, 1195.
32. van Schooneveld, M. M.; Campos-Cuerva, C.; Pet, J.; Meeldijk, J. D.; van Rijssel, J.; Meijerink, A.; Erne, B. H.; de Groot, F. M. F. Composition Tunable Cobalt-Nickel and Cobalt-

Iron Alloy Nanoparticles Below 10 NM Synthesized Using Acetonated Cobalt Carbonyl. *J. Nanopart. Res.* **2012,** *14*.
33. Kang, E.; Park, J.; Hwang, Y.; Kang, M.; Park, J. G.; Hyeon, T. Direct Synthesis of Highly Crystalline and Monodisperse Manganese Ferrite Nanocrystals. *J. Phys. Chem. B* **2004,** *108*, 13932.
34. Hyeon, T.; Lee, S. S.; Park, J.; Chung, Y.; Bin Na, H. Synthesis of Highly Crystalline and Monodisperse Maghemite Nanocrystallites Without a Size-Selection Process. *J. Am. Chem. Soc.* **2001,** *123*, 12798.
35. Meffre, A.; Mehdaoui, B.; Kelsen, V.; Fazzini, P. F.; Carrey, J.; Lachaize, S.; Respaud, M.; Chaudret, B. A Simple Chemical Route toward Monodisperse Iron Carbide Nanoparticles Displaying Tunable Magnetic and Unprecedented Hyperthermia Properties. *Nano Lett.* **2012,** *12*, 4722.
36. Puntes, V. F.; Krishnan, K. M.; Alivisatos, A. P. Colloidal Nanocrystal Shape and Size Control: The Case of Cobalt. *Science* **2001,** *291*, 2115.
37. Huang, L.; Zhang, X. P.; Wang, Q. Q.; Han, Y. J.; Fang, Y. X.; Dong, S. J. Shape-Control of Pt-Ru Nanocrystals: Tuning Surface Structure for Enhanced Electrocatalytic Methanol Oxidation. *J. Am. Chem. Soc.* **2018,** *140*, 1142.
38. Lagunas, A.; Jimeno, C.; Font, D.; Sola, L.; Pericas, M. A. Mechanistic Studies on the Conversion of Dicobalt Octacarbonyl Into Colloidal Cobalt Nanoparticles. *Langmuir* **2006,** *22*, 3823.
39. Puntes, V. F.; Zanchet, D.; Erdonmez, C. K.; Alivisatos, A. P. Synthesis of hcp-Co Nanodisks. *J. Am. Chem. Soc.* **2002,** *124*, 12874.
40. Kang, Y. J.; Murray, C. B. Synthesis and Electrocatalytic Properties of Cubic Mn-Pt Nanocrystals (Nanocubes). *J. Am. Chem. Soc.* **2010,** *132*, 7568.
41. Lee, D. C.; Ghezelbash, A.; Stowell, C. A.; Korgel, B. A. Synthesis and Magnetic Properties of Colloidal MnPt3 Nanocrystals. *J. Phys. Chem. B* **2006,** *110*, 20906.
42. Kang, Y.; Pyo, J. B.; Ye, X.; Diaz, R. E.; Gordon, T. R.; Stach, E. A.; Murray, C. B. Shape-Controlled Synthesis of Pt Nanocrystals: The Role of Metal Carbonyls. *ACS Nano* **2013,** *7*, 645.
43. Lewis, K. E.; Golden, D. M.; Smith, G. P. Organometallic Bond Dissociation Energies: Laser Pyrolysis of $Fe(CO)_5$, $Cr(CO)_6$, $Mo(CO)_6$, and $W(CO)_6$. *J. Am. Chem. Soc.* **1984,** *106*, 3905.
44. Werner, H. Kinetic Studies on Substitution Reactions of Carbonylmetal Complexes. *Angew. Chem. Int. Edit.* **1968,** *7*, 930.
45. Darensbourg, D. J. Mechanistic Pathways for Ligand Substitution Processes in Metal Carbonyls. *Adv. Organomet. Chem.* **1982,** *21*, 113.
46. Angelici, R. J. Kinetics and Mechanisms of Substitution Reactions of Metal Carbonyl Complexes. *Organomet. Chem. Rev.* **1968,** *3*, 173.
47. Atwood, J. D.; Brown, T. L. Cis Labilization of Ligand Dissociation. 3. Survey of Group 6 and 7 Six-Coordinate Carbonyl Compounds. The Site Preference Model for Ligand Labilization Effects. *J. Am. Chem. Soc.* **1976,** *98*, 3160.
48. Howell, J. A. S.; Burkinshaw, P. M. Ligand Substitution-Reactions at Low-Valent 4-Coordinate, 5-Coordinate, and 6-Coordinate Transition-Metal Centers. *Chem. Rev.* **1983,** *83*, 557.
49. Kang, Y. J.; Ye, X. C.; Murray, C. B. Size- and Shape-Selective Synthesis of Metal Nanocrystals and Nanowires Using CO as a Reducing Agent. *Angew. Chem. Int. Edit.* **2010,** *49*, 6156.

50. Wu, B. H.; Zheng, N. F.; Fu, G. Small Molecules Control the Formation of Pt Nanocrystals: A Key Role of Carbon Monoxide in the Synthesis of Pt Nanocubes. *Chem. Commun.* **2011,** *47*, 1039.
51. Darensbourg, D. J.; Pala, M.; Simmons, D.; Rheingold, A. L. Chemical and Structural Characterization of $W(CO)_5OPPh_2NPPh_3$. A Novel Complex Containing a Phosphine Oxide Ligand Derived from the Bis(triphenylphosphine)nitrogen(1+) Cation. *Inorg. Chem.* **1986,** *25*, 3537.
52. Planinić, P.; Meider, H. Synthesis and Characterization of Molybdenum(0) and Tungsten(0) Carbonyl Derivatives of Methylenebis[diphenylphosphine Oxide] And Bis[diphenylphosphinyl)methyl]phenylphosphine Oxide. *Polyhedron* **1989,** *8*, 627.
53. Cook, J. B.; Nicholson, B. K.; Smith, D. W. A structural, spectroscopic and theoretical study of the triphenylphosphine chalcogenide complexes of tungsten carbonyl, $[W(XPPh_3)(CO)_5]$, X = O, S, Se. *J. Organomet. Chem.* **2004,** *689*, 860.
54. Lang, R. F.; Ju, T. D.; Kiss, G.; Hoff, C. D.; Bryan, J. C.; Kubas, G. J. Oxidative Addition of Disulfides to the Complex $W(CO)_3(phen)(EtCN)$. Synthesis, Structure, and Reactivity of $W(CO)_2(phen)(SR)_2$ (R = Ph, Me, CH_2Ph, ^tBu; phen = 1,10-Phenanthroline) Coordinatively Unsaturated Complexes of Tungsten(II) That Reversibly Bind CO and Other Ligands. *Inorg. Chem.* **1994,** *33*, 3899.
55. Lang, R. F.; Ju, T. D.; Kiss, G.; Hoff, C. D.; Bryan, J. C.; Kubas, G. J. Oxidative Addition of Thiols, Disulfides, Iodine, and Hydrogen Iodide to $W(CO)_3(P^iPr_3)_2$. Preparation of Stable 17-Electron Tungsten Thiolate Radicals from Complexes with Weak W-H Bonds. *J. Am. Chem. Soc.* **1994,** *116*, 7917.
56. Fortman, G. C.; Kegl, T.; Hoff, C. D. Kinetic, Thermodynamic, and Mechanistic Aspects of Oxidative Addition Reactions of RE-ER (E = S, Se, Te) and Transition Metal Complexes. *Curr. Org. Chem.* **2008,** *12*, 1279.
57. Fang, Y. Q.; Dong, Q.; Pan, J.; Liu, H. Y.; Liu, P.; Sun, Y. Y.; Li, Q. J.; Zhao, W.; Liu, B. B.; Huang, F. Q. Observation of Superconductivity in Pressurized 2M WSe_2 Crystals. *J. Mater. Chem. C* **2019,** *7*, 8551.
58. Darensbourg, D. J.; Walker, N.; Darensbourg, M. Y. Synthesis of Metal Carbonyl Complexes Highly Enriched in Carbon-13: Utilization of the CO-Labilizing Ability of $(n\text{-}Bu)_3P{=}O$. *J. Am. Chem. Soc.* **1980,** *102*, 1213.
59. Darensbourg, D. J.; Darensbourg, M. Y.; Walker, N. Studies Using $(n\text{-}Bu)_3P{=}O$ as a Carbon Monoxide Labilizing Ligand in the Synthesis of Metal Carbonyl Complexes Highly Enriched in ^{13}CO. *Inorg. Chem.* **1981,** *20*, 1918.
60. Aroney, M. J.; Buys, I. E.; Davies, M. S.; Hambley, T. W. Crystal-Structures of $[W(CO)_5(PPh_3)]$, $[M(CO)_5(AsPh_3)]$ and $[M(CO)_5(SbPh_3)]$ (M = Mo or W): A Comparative Study of Structure and Bonding in $[M(CO)_5(EPh_3)]$ Complexes (E = P, As or Sb; M = Cr, Mo or W). *J. Chem. Soc., Dalton Trans.* **1994**, 2827.
61. Cotton, F. A.; Kraihanzel, C. S. Vibrational Spectra and Bonding in Metal Carbonyls. 1. Infrared Spectra of Phosphine-Substituted Group Vi Carbonyls in Co Stretching Region. *J. Am. Chem. Soc.* **1962,** *84*, 4432.
62. Angelici, R. J.; Malone, M. D. Infrared Studies of Amine Pyridine and Phosphine Derivatives of Tungsten Hexacarbonyl. *Inorg. Chem.* **1967,** *6*, 1731.
63. Cotton, F. A.; Darensbourg, D. J.; Ilsley, W. H. π Acidity of Tris(2-cyanoethyl)phosphine. X-ray Structural Studies of $M(CO)_5P(CH_2CH_2CN)_3$ (M = Cr, Mo) and $Mo(CO)_5P(C_6H_5)_3$. *Inorg. Chem.* **1981,** *20*, 578.

64. Honeychuck, R. V.; Hersh, W. H. Observation of a Novel ^{31}P NMR Cis-Influence Series: Implications for the Relative Basicity of PPh3 and PMe_3 in Tungsten Carbonyl Complexes. *Inorg. Chem.* **1987,** *26*, 1826.
65. Wovkulich, M. J.; Atwood, J. D. Ligand Dissociation From Mono-Substituted Derivatives of Hexacarbonylchromium (Cr(CO)5L, L = $P(C_6H_5)_3$, $P(C_4H_9)_3$, $P(OCH_3)_3$, $P(OC_6H_5)_3$, and $As(C_6H_5)_3$). *J. Organomet. Chem.* **1980,** *184*, 77.
66. Angelici, R. J.; Graham, J. R. Kinetic Studies of Group 6 Metal Carbonyl Complexes. I. Substitution Reactions of Dipyridyl Complexes of Chromium Hexacarbonyl. *J. Am. Chem. Soc.* **1965,** *87*, 5586.
67. Angelici, R. J.; Graham, J. R. Kinetic Studies of Group 6 Metal Carbonyl Complexes. IV. Substitution Reactions of O-Phenanthroline Complexes of Chromium Hexacarbonyl. *Inorg. Chem.* **1967,** *6*, 988.
68. Parker, P. J.; Wojcicki, A. Kinetic Studies of Carbonyl Substitution in Quinolinolatotetracarbonylmanganese(I) and Its Tricarbonyl Derivatives. *Inorg. Chim. Acta* **1974,** *11*, 17.
69. Cotton, F. A.; Darensbourg, D. J.; Kolthammer, B. W. S.; Kudaroski, R. Solid-State and Solution Structures of [PNP][$W(CO)_5O_2CCH_3$] and [PNP][$W(CO)_4(PEt_3)O_2CCH_3$] and the CO-Labilizing Ability of the Acetato Ligand in These Anionic Derivatives. *Inorg. Chem.* **1982,** *21*, 1656.
70. Brown, R. A.; Dobson, G. R. Octahedral Metal Carbonyls. XXI. Carbonyl and Metal–Carbon Stretching Spectra of Monosubstituted Group Vib Metal Carbonyls. *Inorg. Chim. Acta* **1972,** *6*, 65.
71. Fenske, R. F.; Dekock, R. L. Electronic Structure and Bonding in Manganese Pentacarbonyl Halides and Hydride. *Inorg. Chem.* **1970,** *9*, 1053.